Journal of Physics: Conference Series **180** (2009) 012059 doi:10.1088/1742-6596/180/1/012059

Advanced simulation of electron heat transport in fusion plasmas

Z Lin[1], Y Xiao[1], I Holod[1], W Zhang[1], W Deng[1], S Klasky[2], J Lofstead[3], C Kamath[4], and N Wichmann[5]

[1]Department of Physics and Astronomy, University of California, Irvine, CA 92697
[2]Oak Ridge National Laboratory, Oak Ridge, TN 37831
[3]Georgia Institute of Technology, College of Computing, Atlanta, GA 30332
[4]Lawrence Livermore National Laboratory, Livermore, CA 94550
[5]Cray Inc., 411 First Avenue S., Suite 600, Seattle, WA 98104
Email: zhihongl@uci.edu

Abstract. Electron transport in burning plasmas is more important since fusion products first heat electrons. First-principles simulations of electron turbulence are much more challenging due to the multi-scale dynamics of the electron turbulence, and have been made possible by close collaborations between plasma physicists and computational scientists. The GTC simulations of collisionless trapped electron mode (CTEM) turbulence show that the electron heat transport exhibits a gradual transition from Bohm to gyroBohm scaling when the device size is increased. The deviation from the gyroBohm scaling can be induced by large turbulence eddies, turbulence spreading, and non-diffusive transport processes. Analysis of radial correlation function shows that CTEM turbulence eddies are predominantly microscopic but with a significant tail in the mesoscale. A comprehensive analysis of kinetic and fluid time scales shows that zonal flow shearing is the dominant decorrelation mechanism. The mesoscale eddies result from a dynamical process of linear streamers breaking by zonal flows and merging of microscopic eddies. The radial profile of the electron heat conductivity only follows the profile of fluctuation intensity on a global scale, whereas the ion transport tracks more sensitively the local fluctuation intensity. This suggests the existence of a nondiffusive component in the electron heat flux, which arises from the ballistic radial $E \times B$ drift of trapped electrons due to a combination of the presence of mesoscale eddies and the weak de-tuning of the toroidal precessional resonance that drives the CTEM instability. On the other hand, the ion radial excursion is not affected by the mesoscale eddies due to a parallel decorrelation, which is not operational for the trapped electrons because of a bounce averaging process associated with the electron fast motion along magnetic field lines. The presence of the nondiffusive component raises question on the applicability of the usual quasilinear theory for the CTEM electron transport. This is in contrast to the good agreement between the quasilinear transport theory and simulation results of the electron heat transport in electron temperature gradient (ETG) turbulence, which is regulated by a wave-particle decorrelation. Therefore, the transport in the CTEM turbulence is a fluid-like eddy mixing process even though the linear CTEM instability is driven by a kinetic resonance. In contrast, a kinetic process dominates the transport in the ETG turbulence, which is characterized by macroscopic streamers.

1. Introduction

Understanding the physics of the turbulent transport is one of the most important scientific challenges facing magnetically confined, burning plasma experiments, since ignition is sustained by a balance between the heat loss due to the turbulent transport and the self-heating by fusion products. Current reactor design relies on the extrapolation of the transport level from present-day fusion experiments to much larger future devices, such as the International Thermonuclear Experimental Reactor (ITER)[1]. An important goal of predictive simulations is to replace such empirical scalings by first-principles numerical simulations[2].

Turbulence of the fusion plasma in a tokamak reactor is often excited by pressure-gradient-driven, electrostatic, drift-wave instabilities possessing anisotropic mode structures. Turbulence eddies rotate along surfaces of constant electrostatic potentials in the direction perpendicular to both the electric and magnetic fields (so called $E \times B$ drift). In the prevailing fluid picture[3], transport is understood as arising from the eddy mixing of a random walk process with a correlation length of the eddy size and a decorrelation time of the eddy turnover time[4,5]. The mixing length argument[6] conjectures that the transport increases significantly with a larger eddy size along the radial direction of pressure gradients. The concept of turbulent transport via the eddy mixing is valid when the collisional mean-free-path of constituent particles is much shorter than the eddy correlation length so that particles and eddies move together as fluid elements. However, in high temperature fusion plasmas, the mean-free-path of charged particles along the magnetic field lines is much longer than the typical eddy length in the parallel direction. In this nearly-collisionless, wave-dominated plasma turbulence, transport in the radial direction is carried by the random $E \times B$ motions of charged particles. If the charged particles de-couple from the turbulence eddies due to kinetic effects before the eddies can execute a complete rotation, the transport process is regulated by the kinetic wave-particle decorrelation rather than by the fluid eddy mixing. The different transport processes could lead to different transport scaling.

In this study, we examine the relevance of the fluid and kinetic processes in electron heat transport from largest ever fusion simulations resolving the electron dynamics with a real electron-to-ion mass ratio using the gyrokinetic toroidal code (GTC)[5]. Electron transport in fusion plasmas has not been studied as much as the ion transport, but is more important in a burning plasma experiment ITER since the energetic fusion products (α-particles) heat electrons first. Primary candidates for driving electron heat transport in fusion plasmas are the collisionless trapped electron mode (CTEM)[7] and electron temperature gradient (ETG)[8] turbulence. Our first-principles simulations clarify device size scaling, non-diffusive, and non-local turbulent transport. A comparative study between the CTEM and ETG turbulence provides important insights on the dynamics of nonlinear wave-particle interactions and the fluid eddy mixing in regulating the electron heat transport. In particular, the CTEM turbulence is characterized by the co-existence of micro- and meso-scale eddies. The electron heat transport is a fluid-like eddy mixing process even though the linear CTEM instability is driven by a kinetic resonance. In contrast, a kinetic process dominates the transport in the ETG turbulence, which is characterized by macroscopic streamers.

Numerical simulations of the electron turbulence are more challenging due to the small electron-to-ion mass ratio (thus large electron thermal velocity), which introduces smaller spatial scales and faster time scales as compared to the ion turbulence. Global GTC simulation is needed for the multi-scale electron turbulence, which becomes feasible thanks to the implementation of an advanced electron model[9] based on the expansion of electron response using the mass ratio as the small parameter, an efficient global field aligned mesh[10], and a highly scalable algorithm using multi-level parallelisms[11] that enables GTC to efficiently scale up to more than 100,000 cores. These breakthrough simulations with the electron dynamics in the global geometry were carried out in close collaborations with computational scientists in the areas of I/O, parallelization and optimization, workflow, and data

analysis. GTC is currently an early application code for the peta-flop supercomputer at ORNL, a benchmark code for CRAY, part of the benchmark suite at NERSC and part of the code suite for the critical study of applications and architectures designated by DOE ASCR. The scientific importance of GTC simulations for ITER burning plasma experiments is also evident from the selection[12] of GTC simulations by ASCR as the "Top Breakthroughs in Computational Science".

The state-of-the-art GTC simulation of the CTEM turbulence used 28,000 cores for 42 hours and produced 60 TB of data in a dedicated run on jaguar. Simulation results show that the electron heat transport exhibits a gradual transition from Bohm to gyroBohm scaling when the device size is increased[13]. The deviation from the gyroBohm scaling can be induced by large turbulence eddies, turbulence spreading, and non-diffusive transport processes. Analysis of radial correlation function shows that CTEM turbulence eddies are predominantly microscopic but with a significant component in the mesoscale. The macroscopic, linear streamers are mostly destroyed by zonal flow shearing, which is further confirmed by a comprehensive analysis of kinetic and fluid time scales showing that zonal flow shearing is the dominant decorrelation mechanism. The time evolution of the turbulence shows that the mesoscale eddies result from a dynamical process of linear streamers breaking by zonal flows and merging of microscopic eddies. The radial profile of the electron heat conductivity only follows the profile of fluctuation intensity on a global scale, whereas the ion transport tracks more sensitively the local fluctuation intensity. This suggests the existence of a nondiffusive component in the electron heat flux, which arises from the ballistic radial $E \times B$ drift of trapped electrons due to a combination of the presence of mesoscale eddies and the weak detuning of the toroidal precessional resonance that drives the CTEM instability. On the other hand, the ion radial excursion is not affected by the mesoscale eddies due to a parallel decorrelation, which is not operational for the trapped electrons because of a bounce averaging process associated with the electron fast motion along the magnetic field lines. The presence of nondiffusive component raises questions on the applicability of the usual quasilinear theory for the CTEM electron transport. This is in contrast to the good agreement between the quasilinear transport theory and simulation results of the electron heat transport in the ETG turbulence. In the ETG turbulence, wave-particle decorrelation is the dominant mechanism responsible for the electron heat transport[14]. ETG turbulence is dominated by radially elongated eddies (streamers). Various spatial and temporal scales of the ETG turbulence are calculated through comprehensive analysis of the massive data produced from simulations. We find that ETG transport is proportional to the local fluctuation intensity, since phase-space island overlap leads to a diffusive process with a time scale comparable to the wave-particle decorrelation time determined by the parallel spectral width. The kinetic time scale is much shorter than the fluid time scale of eddy mixing.

Our results have important implications on the extrapolation of transport properties from present-day tokamaks to future large reactors and on the choice of time scales in transport models. The transition from Bohm to gyroBohm scaling of the electron heat transport in the CTEM turbulence is favorable for the large fusion reactor ITER. The nonlocal transport properties require a global simulation (instead of a local, flux-tube simulation). The non-diffusive transport in the CTEM turbulence cannot be accurately described by the quasilinear theory underlying most of the existing transport models. The kinetic picture of wave-particle decorrelation for ETG transport is inconsistent with the prevailing picture of fluid eddy mixing. Since the ratio of fluid-to-kinetic time scales increases with the device size, the extrapolation of the transport level from present-day experiments to future larger reactors could be overly pessimistic, if the simplistic mixing length argument with the streamer length as the spatial step size and the fluid time scale as the time step size is invoked.

This paper is organized as follows. The GTC physics and computational models are summarized in Sec. 2. Sec. 3 presents GTC simulation results of the CTEM and ETG instability saturation and fluctuation characteristics. Transport processes in the CTEM and ETG turbulence are discussed in Sec. 4. Sec. 5 is the conclusions.

2. Gyrokinetic Toroidal Code (GTC)

The simulations in this work were carried out using the Gyrokinetic Toroidal Code (GTC), which is a fully global 3D particle-in-cell code developed for first-principle simulations of turbulence and transport in magnetically confined plasmas. We emphasize the global aspect of the simulation in contrast to the local simulation of only a small region, or flux tube, surrounding a chosen magnetic field line.

2.1. Simulation model

We are studying low frequency drift waves characterized by a short wavelength in the direction perpendicular to the magnetic field lines but a very long wavelength in the direction parallel to the field. In the gyrokinetic simulation[15], the phase attribute of the fast gyration (or cyclotron) motion of the charged particles around the magnetic field lines is averaged away, reducing the dimensionality of the system from 6D to 5D. This method[16] removes the fast cyclotron motion, which has a much higher frequency than the characteristic waves of plasma microturbulence.

The particle-in-cell method consists of moving particles along the characteristics of the gyrokinetic equation. The electrostatic potential and field are obtained by solving the Poisson equation on a spatial mesh after gathering the charge density on the grids. The electrostatic forces are subsequently scattered back to the particle positions for advancing the particle orbits. The use of spatial grids and the procedure of gyroaveraging[15] reduce the intensity of small scale fluctuations (particle noise). Particle collisions can be recovered as a "subgrid" phenomenon via Monte Carlo methods. The particle noise is further reduced by using a perturbative simulation method[17] where only the perturbed distribution function is calculated in simulation. Numerical properties of the electron dynamics are improved by an electrostatic fluid-kinetic hybrid electron model[9] based on an expansion of the electron response using the electron–ion mass ratio as a small parameter. Electron response is adiabatic in the lowest order and nonadiabatic response is taken into account in the higher order equations[18].

GTC employs the magnetic coordinates, which provide the most general coordinate system for any magnetic configuration possessing nested surfaces. General geometry with strong shaping has been implemented in GTC using a Poisson solver[19] in real space and a spline fit of the equilibrium data from an MHD code such as EFIT[20]. The property of straight field lines in the magnetic coordinates is most suitable for describing the instability with field aligned eigenmodes and enables the implementation of an efficient global field aligned mesh for the quasi-2D structure of the plasma turbulence in the toroidal geometry[10]. The global field-aligned mesh provides the highest possible computational efficiency without any simplification in terms of physics models or simulation geometry. The magnetic coordinates are also desirable for efficiently integrating the particle orbits, which move predominantly along the magnetic field line direction. The equation of motion can be derived from a Hamiltonian formulation[21] which conserves phase space volume and is best for integrating particle orbits for a long period.

2.2. Parallelization model

GTC employs three levels of parallelism. The original parallel scheme implemented in GTC[5] is a 1D domain decomposition in the symmetric, toroidal direction (long way around the torus) using Message Passing Interface (MPI). Each MPI process is in charge of a toroidal domain with both particles and fields. Particles move from one domain to another while they travel around the torus. All communications are one-way traffic to avoid congestion. A second level of parallelism was later implemented[11] to increase the concurrency. Within each toroidal domain, we now divide the particles between several MPI processes, but each process keeps a copy of all the fields on a single toroidal plane. A "particle-domain" communicator links the MPI processes within a toroidal domain of the

original 1D domain decomposition, while a "toroidal-domain" communicator links in a ring-like fashion all the MPI processes with the same intra-domain rank. To take advantage of the shared memory capability of multi-core nodes, a third level of parallelism is implemented[11] at the loop level using OpenMP compiler directives. These three levels of parallelism using mixed-mode MPI-OpenMP enables GTC to scale to a very large number of processors and use a very large number of particles, which results in a very high phase space resolution and a low statistical noise[22]. Shown in **Fig. 1** is the weak scaling of the GTC computing power, which is almost a linear function of the number of cores up to 100,000 of cores on Cray XT5 supercomputer. GTC is portable and optimized for various scalar and vector supercomputers[11].

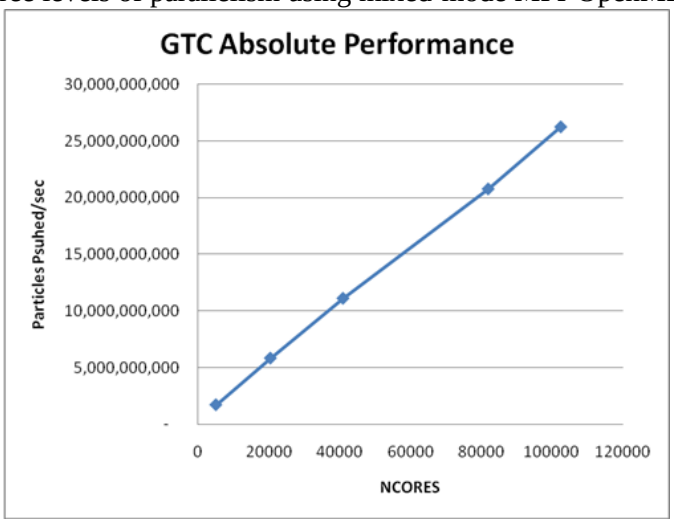

Fig. 1. *Absolute scaling of GTC computing power as a function of number of cores.*

When GTC uses tens of thousands of nodes, having each node create an individual netCDF[23] restart file causes unacceptable delay in the Lustre[24] file system due to the large number of simultaneous file creation requests. To remove this bottleneck, the IO was rewritten to use HDF-5 collectives[25]. To avoid any further changes to the IO layer, we developed an abstraction layer called ADIOS (ADapatable IO System)[26,27] in the collaboration among SciDAC fusion projects GPS-TTBP, CPES, and GSEP[28]. ADIOS provides a simple API that can select automatically the best techniques for each different grouping of data as specified by an entry in an external XML configuration file. To achieve the best performance with any chosen IO method, we have worked with experts on each method, such as synchronous collective MPI-IO[29], HDF-5, and parallel netCDF, to create an optimal implementation. We also have two asynchronous methods of the DART[30] system and DataTap[31]. ADIOS also simplifies the IO routines through an automatic code generation system that can be easily included. By modifying the XML file, all required changes to the IO routines to properly perform the IO can be generated as part of the recompilation without touching the science part of the code. For performance, with the synchronous collective MPI-IO method, we consistently measure a data transfer rate for restarts at 20 GB/s aggregate across the entire system run. Using the DART asynchronous method, it takes 12 seconds to generate 1.2 TB of data.

This concept can be readily generalized for processing data. For example, we can create a method to represent a visualization engine and add it to ADIOS. This method's implementation would incorporate all of the calls, data formatting, setup, and other bits of code necessary for connecting GTC with the visualization engine. The user could then turn on or off the in situ visualization by merely changing the method used for writing a particular grouping of data. For example, the particle data in GTC is a prime candidate for using such a method. If offline visualization is preferred or required for a particular run, the method for particle writes could be changed to something else, for example, MPI-IO. Other advantages of ADIOS include directly integrating workflow through the DataTap and DART systems and even Kepler[32]. While Kepler integration provides a natural interface with existing workflows, these largely rely on files be written to disk in order for the workflow to process. The asynchronous DataTap and DART systems have a similar workflow concept using dynamic code deployment and in stream message passing.

3. Instability saturation and fluctuation characteristics of CTEM and ETG turbulence

The collisionless trapped electron mode (CTEM) instability with a characteristic poloidal wavelength on the order of the ion gyroradius (ρ_i) is driven by the toroidal precessional resonance between trapped electrons and driftwaves. GTC simulations[13] show that this linear CTEM instability is saturated by the shearing effects of the nonlinearly-generated zonal flows. This is further confirmed by a comprehensive analysis of kinetic and fluid time scales showing that zonal flow shearing is the dominant decorrelation mechanism. As a result, the macroscopic, linear, radial streamers are mostly broken by the zonal flows. As shown in the top panel of **Fig. 2** for the contour plot of the electrostatic potential ϕ in a tokamak with a minor radius a=250ρ_i, the steady state turbulence is dominated by microscopic eddies with a scale length of 5ρ_i, but with also a significant component of mesoscale (5-50ρ_i) streamers. The mesoscale eddies result from a dynamical process of zonal flow breaking of linear streamers and spontaneous merging of microscopic eddies. For the following analysis of space and time scales, we use the fluctuation data from a simulation of tokamak size of a=500ρ_i. To quantify the perpendicular structures, we calculate the two-point correlation function, $C_{r\zeta}(\Delta r,\Delta\zeta)=\dfrac{\langle\phi(r+\Delta r,\zeta+\Delta\zeta)\phi(r,\zeta)\rangle}{\sqrt{\langle\phi^2(r+\Delta r,\zeta+\Delta\zeta)\rangle\langle\phi^2(r,\zeta)\rangle}}$, where $\langle\cdots\rangle$ represents averaging over toroidal ζ and radial r directions at a poloidal angle θ=0. Radial correlation function $C_r(\Delta r)$ is then calculated by taking the maximal value along the ridge of $C_{r\zeta}(\Delta r, \Delta\zeta)$. The function $C_r(\Delta r)$ decays exponentially for the small radial separation but possesses a significant mesoscale tail in the range of 5-50ρ_i. An exponential fit of the initial drop of $C_r(\Delta r)$ gives the short length scale as L_r~5ρ_i. This is the average radial size for the microscopic eddies. The perpendicular structure of the CTEM turbulence is thus multi-scale.

For comparison, the instability saturation and fluctuation characteristics of the electron temperature gradient (ETG) turbulence are quite different. The ETG instability with a much shorter characteristic poloidal wavelength on the order of the electron gyroradius (ρ_e) is driven by electron parallel resonance. The nonlinear saturation of the ETG instability is primarily due to a nonlinear toroidal mode coupling[33]. In this process, the spectral energy successively flows toward longer wavelengths, eventually down to damped modes. The effects of zonal flows in the ETG turbulence are very weak. Therefore, the ETG turbulence after saturation is dominated by macroscopic radial streamers as shown in the lower panel of **Fig. 2** for the contour plot of the electrostatic potential ϕ in a much smaller tokamak with a minor radius of 500ρ_e. The perpendicular structure of the ETG turbulence is thus strongly anisotropic. In the steady state, the ETG turbulence is also mediated by a radial spreading[34] where small scale turbulence eddies are generated in the unstable region (around r=0.5a) and flow along the nonlinearly generated radial streamers to the stable region (near r=0 and r=a). Meanwhile, the streamers can break and reconnect, resulting in a very complex dynamical evolution.

The 2D structures on a poloidal plane (perpendicular to the magnetic field lines) shown in **Fig. 2** is extended along the magnetic field lines (in the toroidal direction), resulting in a flux-tube like eddy structures. The parallel wavevector of both CTEM and ETG is $k_{||}$~1/qR, where R is the major radius and q is the safety factor of the tokamak. The radial variations of q cause the eddy structures to twist around in the toroidal direction.

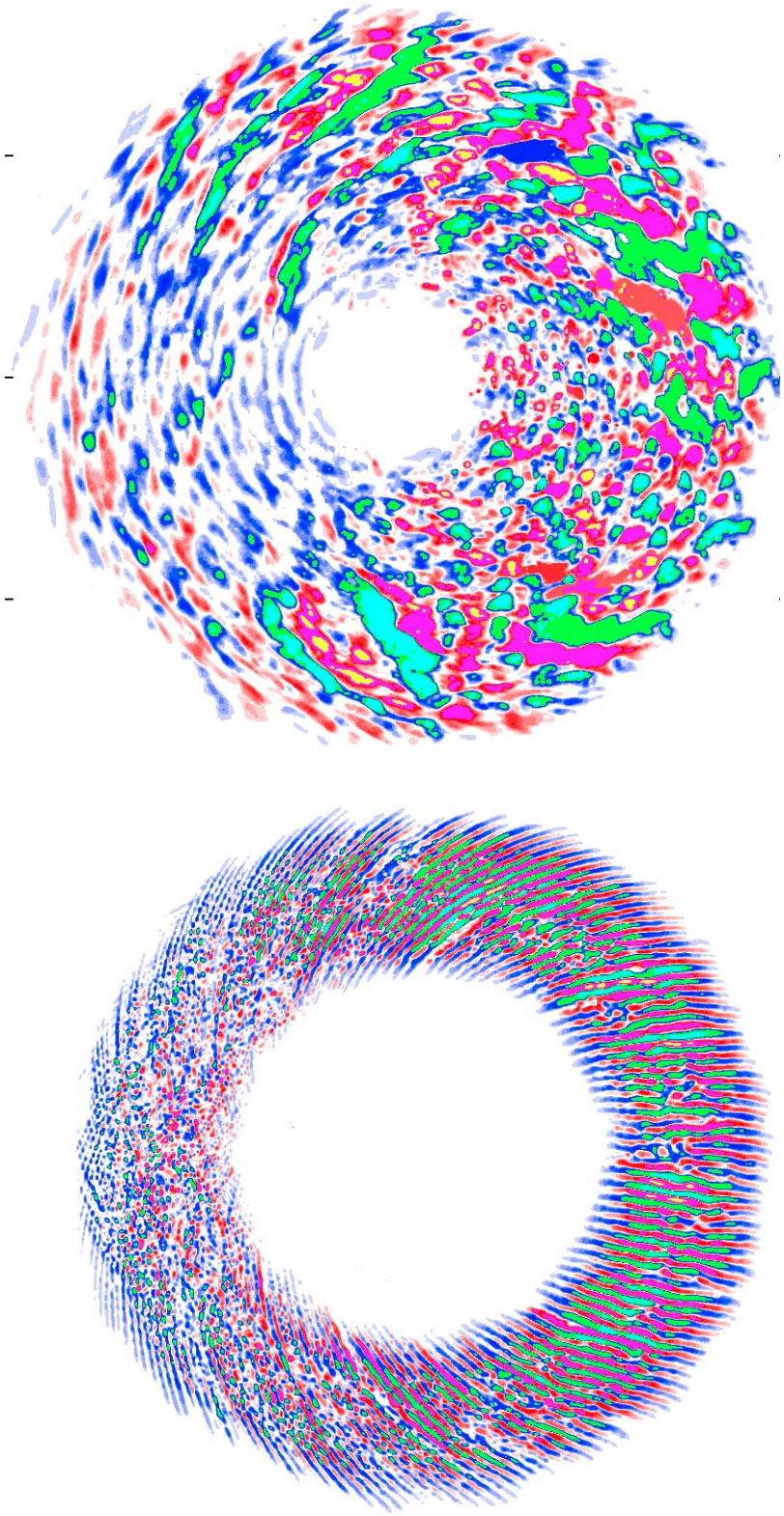

Fig. 2. *Poloidal contour plots of the electrostatic potential ϕ in the CTEM turbulence (top panel) and the ETG turbulence (lower panel).*

4. Transport processes of CTEM and ETG turbulence

To study the transport mechanism, we examine the correlation between heat conductivity to the local turbulence intensity and compare various characteristic time and spatial scales. In the CTEM turbulence[13], the time and flux-surface-averaged ion heat flux $\boldsymbol{Q_i}$, electron heat flux $\boldsymbol{Q_e}$, and radial ExB drift intensity I during the nonlinear stage is shown in the lower right panel of **Fig. 3**. The radial profile of the fluctuation intensity I contains a global envelope plus an oscillating part with a spatial period of ~10ρ_i. The correlation between the radial profiles of the fluctuation intensity I and the ion heat flux $\boldsymbol{Q_i}$ suggests that the ion heat transport is driven by the local $E \times B$ drift intensity I. On the other hand, the radial profile of the electron heat flux $\boldsymbol{Q_e}$ is much smoother and lacks the small scale oscillations. Nonetheless, the global profile is quite similar to the global envelope of the fluctuation intensity I. This suggests that the electron heat transport is close to diffusive on the global scale, but not on the microscopic and meso-scale. The remarkable similarity between the ion heat flux $\boldsymbol{Q_i}$ (top left panel**)** and the fluctuation intensity I (top right panel**)** in both radial structure and time evolution further confirms that the ion heat transport is driven by the local fluctuation intensity. However, the electron transport demonstrates a ballistic propagation in the radial direction (lower left panel**)**. Therefore, the electron heat transport follows the global structure of of $E \times B$ profile but contains a non-diffusive component on the mesoscale.

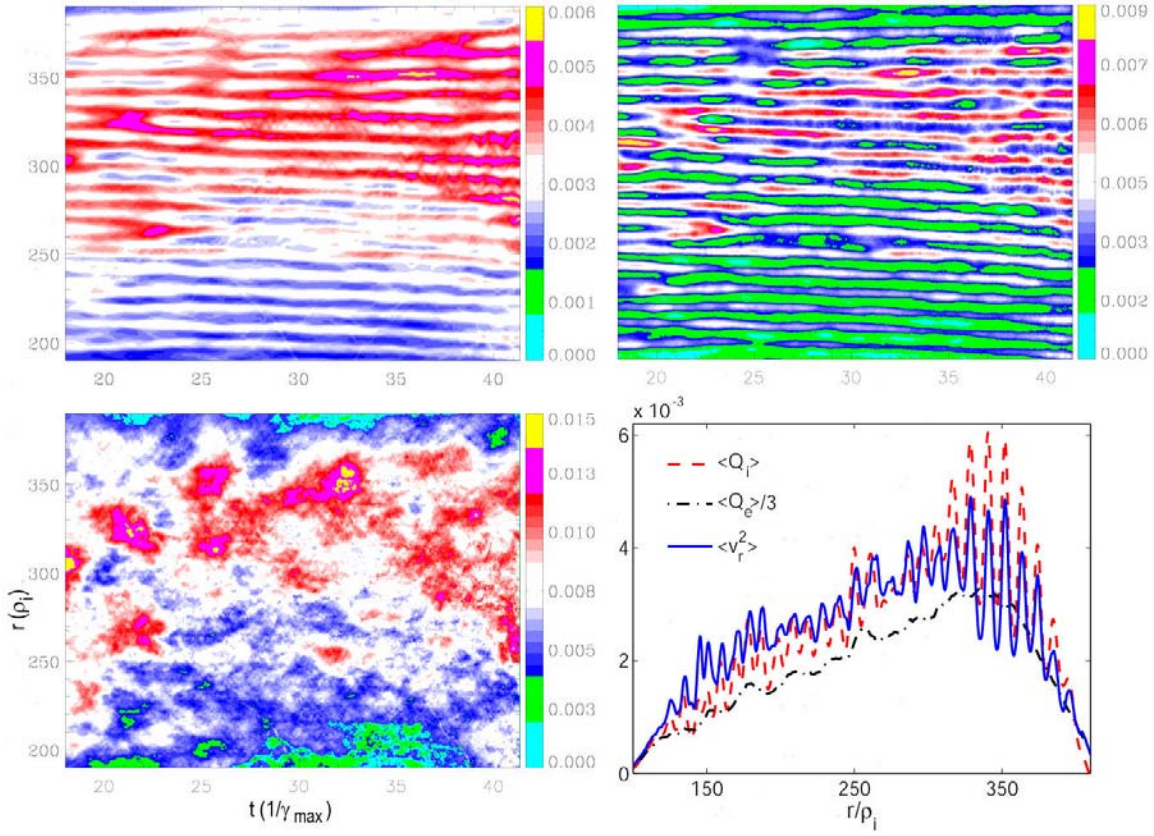

Fig. 3 *Time-radial contour plot for CTEM turbulence intensity (I, top right), ion heat flux (Q_i, top left), electron heat flux (Q_e, lower left), and the radial profiles of the time-averaged I, Q_i,, and Q_e (Lower right panel)*

We can now define an effective wave-particle decorrelation time τ_{wp} since the electron heat transport is proportional to the fluctuation intensity on the global scale, i.e., $\tau_{wp}=2D/I$. Because the particle diffusivity is much smaller than the thermal conductivity, a test particle diffusivity D can be related to the thermal conductivity χ_e by $D = 2\ \chi_e/3$. We find $\tau_{wp}=0.61L_{ne}/v_i$ for the trapped electrons. This characteristic time reflects the physical process relevant to the transport mechanism[14]. To evaluate various time scales, we first calculate the two-time-two-point correlation function $C_{t\zeta}(\Delta t,\Delta\zeta)=\dfrac{\langle\phi(t+\Delta t,\zeta+\Delta\zeta)\phi(t,\zeta)\rangle}{\sqrt{\langle\phi^2(t+\Delta t,\zeta+\Delta\zeta)\rangle\langle\phi^2(t,\zeta)\rangle}}$. Then we calculate the Lagrangian time correlation function $C_t(\Delta t)$ by taking the maximal value along the ridge of $C_{t\zeta}(\Delta t, \Delta\zeta)$, i.e., moving with the wave phase velocity. This Lagrangian time correlation function $C_t(\Delta t)$ decays exponentially with an autocorrelation time $\tau_{auto}=11L_{ne}/v_i$. The eddy turnover time τ_{eddy}, which describes how fast the eddy rotates due to the $E\ X\ B$ drift without the zonal flow shearing, is $\tau_{eddy}=L_r/<\delta v_r>=1.6L_{ne}/v_i$ for microscopic eddies. Another fluid time scale that relates to the dynamics of the turbulence eddies is the zonal flow shearing time, $\tau_s=0.66L_{ne}/v_i$.

The kinetic time scales related to the linear CTEM eigenmode include the wave-particle decorrelation time scales for the trapped electrons to cross the turbulence eddies in the parallel and perpendicular directions. Because of the fast bounce motion, which averages out the parallel electric field, the trapped electrons cannot decorrelate from the wave in the parallel direction. In the spectral range of interest, the CTEM frequency is proportional to the toroidal mode number (i.e., non-dispersive). Thus the resonant electrons cannot decorrelate from the wave in the toroidal direction. On the other hand, the resonant electrons can decorrelate from the wave in the radial direction due to the radial dependence of the precessional frequency. However, this dependence is very weak (on the device size scale). Therefore, the radial de-tuning time is also very long. Trapped electrons thus remain resonant with the wave until they are diffused nonlinearly across the turbulence eddies. This nonlinear kinetic time scale is the resonance broadening time τ_{rb}, which is calculated as $\tau_{rb}=5.1L_{ne}/v_i$. Therefore, all kinetic time scales are much longer than the fluid time scales, i.e., CTEM transport is a fluid-like process.

The physical picture of the device size scaling of the electron heat transport in the CTEM turbulence thus emerges from the combination of the turbulence structures and the fluid-like nature of the electron transport process. The resonant trapped electrons can be convected by the $E\ X\ B$ drift across the large number of mesoscale eddies. This mesoscale ballistic process then drives a non-diffusive component in the electron heat transport and smooths small radial scale structure of the turbulence intensity. The mesoscale ballistic electron heat flux, together with the turbulence spreading, leads to the deviation from the gyroBohm transport scaling for the small devices. The electron heat transport thus exhibits a device size scaling characterized by a gradual transition from Bohm to gyroBohm scaling, which is good news for the large fusion reactor ITER.

In contrast, we find that stochastic wave-particle decorrelation[14] is the dominant mechanism responsible for the electron heat transport driven by the ETG turbulence with extended radial streamers. The phase-space island overlap due to the interactions of many toroidal modes leads to a diffusive transport process with a time scale comparable to the wave-particle decorrelation time, determined by the parallel spectral width. This kinetic time scale of the wave-particle decorrelation is much shorter than the fluid time scales of the eddy mixing. Consistently, the transport is proportional to the local fluctuation intensity, and quasilinear calculation of the electron heat conductivity using measured spectra agrees well with the simulation value[14].

5. Conclusions

Large scale simulations of electron heat transport in fusion plasmas find that the transport in the collisionless trapped electron mode (CTEM) turbulence is a fluid-like eddy mixing process even though the linear CTEM instability is driven by a kinetic resonance. In contrast, a kinetic process dominates the transport in the electron temperature gradient (ETG) turbulence, which is characterized by macroscopic streamers. The GTC simulations have identified, for the first time, the nonlinear transport processes that determine the level and scaling of the electron transport in fusion plasmas.

Acknowledgments: This work is supported by SciDAC GPS-TTBP, GSEP, and CPES centers. We acknowledge fruitful discussions with C. S. Chang, L. Chen, P. H. Diamond, S. Ethier, T. S. Hahm, and F. Zonca. Simulations used supercomputers at ORNL and NERSC.

References

[1] http://www.iter.org/.
[2] W. M. Tang, *Journal of Physics: Conference Series* **125,** 012047(2008).
[3] A. Hasegawa and K. Mima, *Phys. Fluids* **21**, 87 (1978).
[4] H. Biglari, P. H. Diamond, and P. W. Terry, *Phys. Fluids* B **2**, 1 (1990).
[5] Z. Lin *et al*, *Science* **281**, 1835 (1998).
[6] B. B. Kadomtsev, *Plasma Turbulence* (Academic, London, 1965).
[7] J. Adam, W. Tang, and P. Rutherford, Phys. Fluids **19**, 561 (1976).
[8] W. Horton, B. G. Hong, and W. M. Tang, *Phys. Fluids* **31**, 2971 (1988).
[9] Z. Lin and L. Chen, Phys. Plasmas **8**, 1447 (2001).
[10] Z. Lin *et al*, *Phys. Rev. Lett.* **88**, 195004 (2002).
[11] S. Ethier, W. M. Tang, and Z. Lin, *Journal of Physics: Conference Series* **16**, 1 (2005).
[12] SciDAC Review, special issue 2009, http://www.scidacreview.org/0901/.
[13] Y. Xiao and Z. Lin, submitted to *PRL*.
[14] Z. Lin *et al*, *Phys. Rev. Lett.* **99**, 265003 (2007).
[15] W. W. Lee, *Phys. Fluids* **26**, 556 (1983); *J. Comput. Phys.* **72**, 243 (1987).
[16] A. J. Brizard and T. S. Hahm, *Rev. Mod. Phys.* **79**, 421 (2007).
[17] S. E. Parker and W. W. Lee, *Phys. Fluids* B **5**, 77 (1993).
[18] I. Manuilskiy and W. W. Lee, *Phys. Plasmas* **7**, 1381 (2000).
[19] Z. Lin and W. W. Lee, *Phys. Rev. E* **52**, 5646 (1995).
[20] L. L. Lao *et al*, *Nuclear Fusion* **25**, 1611 (1985).
[21] R. B. White and M. S. Chance, *Phys. Fluids* **27**, 2455 (1984).
[22] I. Holod and Z. Lin, *Phys. Plasmas* **14**, 032306 (2007).
[23] http://www.unidata.ucar.edu/software/netcdf/.
[24] http://www.lustre.org/.
[25] http://hdf.ncsa.uiuc.edu/products/hdf5/.
[26] J. Lofstead, S. Klasky, H. Abbasi, and K. Schwan, in Supercomputing'07, Reno, 2007.
[27] J. Lofstead, F. Zheng, S. Klasky, and K. Schwan, "*Adaptable, Metadata Rich IO Methods for Portable High Performance IO*", in Proceedings of IPDPS'09, Rome, 2009.
[28] http://www.scidac.gov/fusion/fusion.html.
[29] http://www.llnl.gov/icc/lc/siop/mpiio.html.
[30] C. Docan, M. Parashar, and S. Klasky, "*High Speed Asynchronous Data Transfers on the Cray XT3"*. Technical report, Rutgers, The State University of New Jersey, 2007.
[31] K. Schwan, H. Abbasi, M. Wolf, "*Live data workspace: A flexible, dynamic and extensible platform for petascale applications*". In ClusterComputing, Austin, 2007.
[32] http://kepler-project.org/.
[33] Z. Lin, L. Chen, and F. Zonca, *Phys. Plasmas* **12**, 056125 (2005).
[34] Z. Lin and T. S. Hahm, *Phys. Plasmas* **11**, 1099 (2004).